

## Face-to-Face and Edge-to-Face $\pi$ - $\pi$ Interactions in a Synthetic DNA Hairpin with a Stilbenediether Linker

Martin Egli,<sup>\*,†</sup> Valentina Tereshko,<sup>†</sup> Garib N. Mushudov,<sup>‡</sup> Ruslan Sanishvili,<sup>§</sup>  
Xiaoyang Liu,<sup>||</sup> and Frederick D. Lewis<sup>||</sup>

Contribution from the Department of Biological Sciences, Vanderbilt University, Nashville, Tennessee 37235, Structural Biology Laboratory, Department of Chemistry, University of York, Heslington, York YO10 5YW, United Kingdom, Biosciences Division, Argonne National Laboratory, Argonne, Illinois 60439, and Department of Chemistry, Northwestern University, Evanston, Illinois 62008

Received April 9, 2003; E-mail: martin.egli@vanderbilt.edu

**Abstract:** Synthetic conjugates possessing bis(2-hydroxyethyl)stilbene-4,4'-diether linkers (Sd2) form the most stable DNA hairpins reported to date. Factors that affect stability are length and flexibility of the linkers and  $\pi$ -stacking of the stilbene moiety on the adjacent base pair. The crystal structure of the hairpin d(GT<sub>4</sub>G)-Sd2-d(CA<sub>4</sub>C) was determined at 1.5 Å resolution. The conformations of the two molecules in the asymmetric unit differ both in the linker and the stem portions. One of them shows a planar stilbene that is stacked on the adjacent G:C base pair. The other displays considerable rotation between the phenyl rings and an unprecedented edge-to-face orientation of stilbene and base pair. The observation of considerable variations in the conformation of the Sd moiety in the crystal structure allows us to exclude restriction of motion as the reason for the absence of Sd photoisomerization in the hairpins. Conformational differences in the stem portion of the two hairpin molecules go along with different Mg<sup>2+</sup> binding modes. Most remarkable among them is the sequence-specific coordination of a metal ion in the narrow A-tract minor groove. The crystal structure provides unequivocal evidence that a fully hydrated Mg<sup>2+</sup> ion can penetrate the narrow A-tract minor groove, causing the groove to further contract. Overall, the structural data provide a better understanding of the origins of hairpin stability and their photochemical behavior in solution.

### Introduction

Duplex DNA exhibits structural polymorphism, existing in A-, B-, and Z-type structures.<sup>1</sup> In all three structures, adjacent base pairs adopt a parallel  $\pi$ -stacked, face-to-face geometry. Similarly, molecules which intercalate between adjacent base pairs in DNA do so with a  $\pi$ -stacked geometry.<sup>2</sup> We previously reported the structure of a hairpin-forming nucleic acid conjugate in which a stilbene diether linker connects short complementary oligonucleotides.<sup>3</sup> In this low-resolution structure the planar stilbene is also  $\pi$ -stacked with the adjacent base pair. Whereas duplex DNA has a propensity for the formation of  $\pi$ -stacked structures, the aromatic rings in simple organic molecules and in proteins often display a preference for edge-to-face or T-shaped geometries.<sup>4</sup> High-level electronic structure calculations for the benzene dimer indicate that offset face-to-face and edge-to-face geometries have similar energies.<sup>5</sup> This suggests

the possibility of a new type of structural polymorphism in systems having interacting planar aromatic molecules, the existence of both edge-to-face and face-to-face structural isomers. We report here the ability of a B-DNA base pair to engage in edge-to-face as well as face-to-face geometries.

Nucleic acid conjugates in which synthetic linkers connect short complementary oligonucleotides form DNA or RNA hairpins, some of them exhibiting higher stability than their natural counterparts with nucleotide loops.<sup>6-9</sup> DNA hairpins with stilbenedicarboxamide (Sa) linkers showed exceptionally high stability.<sup>10</sup> Thus, stable structures were formed by hairpins with as few as three T:A or two C:G base pairs. The Sa linker excited singlet state acts as selective electron acceptor which oxidizes G, but not the other DNA bases. This property allowed investigation of hole injection and migration processes in the synthetic DNA hairpins.<sup>11</sup> DNA hairpins capped by stilbene-

<sup>†</sup> Vanderbilt University.

<sup>‡</sup> University of York.

<sup>§</sup> Argonne National Laboratory.

<sup>||</sup> Northwestern University.

- (1) Arnott, S. In *Oxford Handbook of Nucleic Acid Structure*; Neidle, S., Ed.; Oxford University Press: Oxford, 1999; pp 1-38.
- (2) Bloomfield, V. A.; Crothers, D. M.; Tinoco, L., Jr. *Nucleic Acids, Structures, Properties, Functions*; University Science Books: Sausalito, CA, 2000.
- (3) Lewis, F. D.; Liu, X.; Wu, Y.; Miller, S. E.; Wasielewski, M. R.; Letsinger, R. L.; Sanishvili, R.; Joachimiak, A.; Tereshko, V.; Egli, M. *J. Am. Chem. Soc.* **1999**, *121*, 9905-9906.
- (4) Hunter, C. A. *Chem. Rev.* **1994**, *23*, 101-110.

- (5) Sinnokrot, M. O.; Valeev, E. F.; Sherrill, C. D. *J. Am. Chem. Soc.* **2002**, *124*, 10887-10893.
- (6) Bevers, S.; Schutte, S.; McLaughlin, L. M. *J. Am. Chem. Soc.* **2000**, *122*, 5905-5915.
- (7) Ma, M. Y. X.; McCallum, K.; Climie, S. C.; Kuperman, R.; Lin, W. C.; Sumner-Smith, M.; Barnett, R. W. *Nucleic Acids Res.* **1993**, *21*, 2585-2589.
- (8) Salunkhe, M.; Wu, T.; Letsinger, R. L. *J. Am. Chem. Soc.* **1992**, *114*, 8768-8772.
- (9) Durand, M.; Chevie, K.; Chassignol, M.; Thuong, N. T.; Maurizot, J. C. *Nucleic Acids Res.* **1990**, *18*, 6353-6359.
- (10) Letsinger, R. L.; Wu, T. *J. Am. Chem. Soc.* **1995**, *117*, 7323-7328.
- (11) Lewis, F. D.; Wu, Y.; Liu, X. *J. Am. Chem. Soc.* **2002**, *124*, 12165-12173.

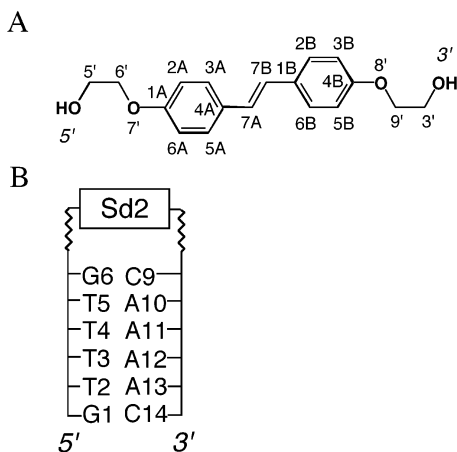


**Figure 1.** (A) Structure and atom numbering of the Sd2 linker. (B) Stem residues are numbered G1, T2, T3, T4, T5, and G6 in strand 1 and C9, A10, A11, A12, A13 and C14 in strand 2, and the Sd2 linker is residue 7.

diether moieties (Sd) are even more stable than those with Sa linkers and constitute the most stable hairpins discovered to date.<sup>3</sup> For example, the hairpin formed by two C:G base pairs linked by a bis(2-hydroxyethyl)-stilbene-4,4'-diether (Sd2; Figure 1) melts at  $>80$  °C in a buffered solution containing 0.1 M NaCl. The singlet state of the Sd linker is an electron donor which can reduce either T or C, but not A or G. Sd-capped hairpins display strongly reduced fluorescence compared to the free stilbenediether, consistent with electron-transfer quenching in the former. However, in hairpins that contain one or more G:C base pairs adjacent to the Sd linker the fluorescence is markedly stronger.<sup>3</sup> Similarly, the efficiency of trans-to-cis photoisomerization is strongly reduced in the Sd-capped hairpins compared to that in the free Sd.

To learn more about the structural properties of a DNA duplex with an Sd2 linker and the conformation of the linker itself, we determined the crystal structure of d(GT<sub>4</sub>G)–Sd2–d(CA<sub>4</sub>C) at 1.5 Å resolution. In the present contribution we will refer to this crystal form as hp15. The structural data demonstrate that the geometry of Sd2 is relatively unrestrained and that the ethoxy tethers allow both face-to-face and edge-to-face orientations between *trans*-stilbene and neighboring base pair. Thus, the two independent molecules (designated hp15-1 and hp15-2 here) constituting the crystallographic asymmetric unit adopt different conformations. In the hairpin with an edge-to-face orientation of Sd2 (hp15-2), the stilbene itself exhibits a significant deviation from planarity. The conformational variations between independent subunits observed in the high-resolution crystal form differ strongly from the situation in a second crystal form whose structure had previously been determined to 3.2 Å resolution.<sup>3</sup> In that crystal form (referred to as hp32 in this work), the conformations of the four subunits (designated hp32-1 to hp32-4) were more uniform, and all four exhibited stacking of the Sd2 unit on the adjacent G:C base pair. In addition to providing new insights into the overall conformation of Sd2-linked DNA hairpins and various orientations of the stilbenediether, hp15-1 and hp15-2 allow the most detailed look to date at the geometry of an A<sub>n</sub>T<sub>n</sub> type A-tract based on crystallographic data. For example, the A-tract minor groove of hp15-1 contracts due to insertion of a hydrated Mg<sup>2+</sup> ion relative to the minor grooves of hp15-2 and the hp32 molecules.

**Table 1.** Selected Crystal Data and Refinement Parameters

parameter	hp15
space group	<i>P</i> 2 <sub>1</sub> 2 <sub>1</sub> 2 <sub>1</sub>
cell constants (Å)	<i>a</i> = 29.89, <i>b</i> = 41.86, <i>c</i> = 51.10
wavelength (Å)	1.000
resolution <sup>a</sup> (Å)	15.0–1.50 (1.539–1.50)
unique reflections (no $\sigma$ cutoff)	9590 (637)
completeness (%)	93.9
redundancy	6.8
<i>R</i> <sub>sym</sub> <sup>b</sup> (%)	4.5
no. of DNA atoms, waters	711, 170
metal ions	5 Mg <sup>2+</sup>
<i>R</i> -work <sup>c</sup> , <i>R</i> -test <sup>d</sup> (%)	20.4 (17.6), 23.9 (27.5)
r.m.s. dist. (Å), angles (deg)	0.017, 1.98

<sup>a</sup> Values in parentheses refer to data in the highest resolution shell. <sup>b</sup>  $R_{\text{sym}} = \sum_{hkl} \sum_i |I(hkl)_i - \langle I(hkl) \rangle| / \sum_{hkl} \sum_i I(hkl)_i$ . <sup>c</sup>  $R = \sum_{hkl} |F(hkl)_o - F(hkl)_c| / \sum_{hkl} F(hkl)_o$ . <sup>d</sup> For 5% of the data.<sup>16</sup>

Here we describe the high-resolution structure, compare the geometries of hp15-1 and hp15-2 to each other and to those of the Sd2-linked DNA hairpins in the earlier low-resolution structure,<sup>3</sup> and conduct a qualitative correlation between the structural results and the thermodynamic stability and efficiency of electron transfer in Sd2–oligodeoxynucleotide conjugates.

## Experimental Section

**Synthesis, Crystallization, and Data Collection.** The d(GT<sub>4</sub>G)–Sd2–d(CA<sub>4</sub>C) hairpin was synthesized and purified as previously described.<sup>3,11</sup> Crystallization was achieved by the hanging drop vapor diffusion technique. A droplet (10  $\mu$ L) containing 1 mM Sd2-linked DNA, 40 mM MgCl<sub>2</sub>, and 8% MPD in 40 mM sodium cacodylate buffer (pH 6) was equilibrated against a reservoir of 40% 2-methyl-2,4-pentanediol (MPD; 1 mL). A single crystal was frozen without further cryoprotection and used for data collection. Separate low- and high-resolution data sets were collected on the insertion device beam line of the SBC-CAT at sector 19 of the APS, Argonne, IL. All data were integrated and scaled with DENZO and SCALEPACK,<sup>12</sup> respectively, and selected crystal data and data collection parameters are summarized in Table 1.

**Structure Determination and Refinement.** The structure of hp15 was determined by the Molecular Replacement technique using the program AMoRe.<sup>13</sup> The hp32-1 molecule of the low-resolution structure<sup>3</sup> served as a starting model. Rigid-body, positional refinement, and simulated annealing were performed in CNS.<sup>14</sup> Restrained anisotropic temperature-factor and final positional refinement were completed with the program REFMAC,<sup>15</sup> using standard values for bulk solvent parameters. *R*-free was monitored by setting aside 5% of the reflection as a test set.<sup>16</sup> An example of the final electron density is depicted in Figure 2 and selected refinement parameters are listed in Table 1.

**Coordinates.** Coordinates and structure factors have been deposited in the Research Collaboratory for Structural Biology (<http://www.rcsb.org>): PDB ID code 1PUY.

## Results and Discussion

**Overall Structure.** The duplex portions of the two independent molecules in the hp15 crystal form exhibit B-form geometry (Figure 3A,B). The hp15-1 molecule has average values for inclination, rise, and twist of  $-0.3^\circ$ , 3.25 Å, and 36.1°,

(12) Otwinowski, Z.; Minor, W. *Methods Enzymol.* **1997**, *276*, 307–326.

(13) Navaza, J. *Acta Crystallogr., Sect. A* **1994**, *50*, 157–163.

(14) Brünger, A. T.; Adams, P. D.; Clore, G. M.; DeLano, W. L.; Gros, P.; Grosse-Kunstleve, R. W.; Jiang, J. S.; Kuszewski, J.; Nilges, M.; Pannu, N. S.; Read, R. J.; Rice, L. M.; Simonson, T.; Warren, G. L. *Acta Crystallogr., Sect. D* **1998**, *54*, 905–921.

(15) Mushudov, G. N.; Vagin, A. A.; Dodson, E. J. *Acta Crystallogr., Sect. D* **1997**, *53*, 240–255.

(16) Brünger, A. T. *Nature* **1992**, *355*, 472–475.

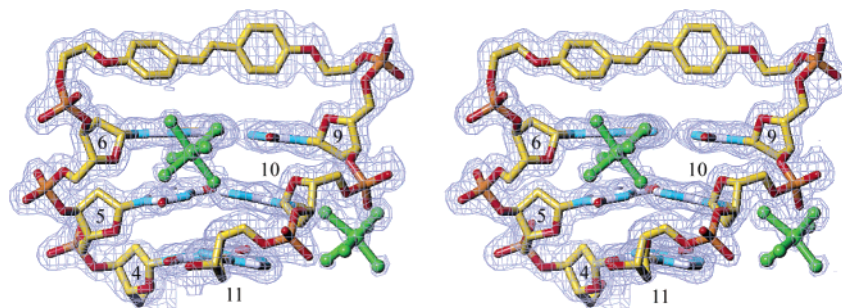


**Figure 2.** Quality of the structure. Stereo diagram of the final Fourier  $2F_o - F_c$  sum electron density at 1.50 Å resolution and contoured at  $1 \sigma$  around residues T4, T5, G6, Sd2, C9, A10, and A11 from hp15-2. The view is into the minor groove, and DNA and Sd2 atoms are colored yellow, red, blue, and orange for carbon, oxygen, nitrogen, and phosphorus, respectively. Two magnesium hexahydrate complexes coordinating in the minor groove (Mg208) and to the backbone (Mg315), respectively, are shown in green.

respectively (calculated with the program CURVES<sup>17</sup>). The average values for these parameters in the second molecule are  $0.5^\circ$ , 3.33 Å, and  $34.6^\circ$ , respectively. In both molecules the inclination is largest for the terminal G1:C14 base pair (hp15-1:  $-8.5^\circ$ ; hp15-2:  $-10.6^\circ$ ). In hp15-1, this base pair also displays the strongest buckle ( $-13.3^\circ$ ; av  $-7^\circ$ ). By comparison, in hp15-2 the buckle is maximal in base pair T2:A13 ( $-14.4^\circ$ ; av  $-8.1^\circ$ ). Except for base pairs G6:C9 adjacent to the Sd2 linker, all base pairs in the two molecules exhibit considerable propeller twists (hp15-1: av  $-13.9^\circ$ ; hp15-2: av  $-13.3^\circ$ ).

Additional differences between the conformations of the six-base pair stems in hp15-1 and hp15-2 are found at the level of the sugar–phosphate backbone. In hp15-1 the pucker of residue G1 is  $C3'$ -endo, with all other sugars adopting either  $C2'$ -endo (eight residues) or  $C1'$ -exo pucker (three residues). In hp15-2 the puckers of both G1 and T2 are of the  $C3'$ -endo type, with the remaining ones adopting  $C2'$ -endo (four residues),  $C1'$ -exo (five residues), or  $C3'$ -exo pucker (A10). These individual differences add up to a root-mean-square (rms) deviation of 1.08 Å between the stem portions of hp15-1 and hp15-2. However, the most drastic conformational differences between the two molecules occur in the Sd2 linker region (Figure 3). The orientations of the stilbene moieties relative to the stem, the geometries of the *trans*-stilbenes as well as the conformations of the ethoxy tethers show considerable deviations. The overall rms deviation between hp15-1 and hp15-2 amounts to 1.26 Å. By comparison, the four independent molecules per asymmetric unit in the hp32 crystal form display a more uniform geometry, with only small differences between the relative orientations of Sd2 linkers and base pairs G6:C9 (Figure 3B).

**Conformations, Intramolecular Interactions, and Energetics of Sd2 Linkers.** The most striking feature of the high-resolution hp15 structure is the conformation of the Sd2 linker and its relative orientation to the neighboring G6:C9 base pair in the hp15-2 molecule (Figure 3). The stilbene in hp15-2 exhibits significant nonplanarity, and the dihedral angle between phenyl rings is  $33^\circ$  (Figure 3C, red). Phenyl ring A attached to the 3'-end of G6 is unstacked and shifted away from the guanine plane. Phenyl ring B is virtually perpendicular to the base of C9, and two of its carbons (5B and 6B) are in van der Waals contact with the cytosine (distances 3.56 and 3.43 Å, respectively). In the hp15-1 molecule, the stilbene is practically planar, with the dihedral angle between phenyls amounting to  $9^\circ$  (Figure

3C, cyan). The *trans* double bond as well as ring A are stacked on G6, and ring B more or less overlaps with the base of C9. The average distance between stilbene atoms and the best plane through the G6:C9 base pair is 3.46 Å.

The phenyl–phenyl dihedral angle in hp15-2 is similar to that for a stilbene-4,4-dicarboxamide which packs in a one-dimensional tape in which amide–amide hydrogen bonding holds adjacent stilbenes at a fixed separation of 5 Å.<sup>18</sup> The parent *trans*-stilbene is planar in the solid state,<sup>19</sup> but nonplanar with a phenyl–phenyl dihedral angle of ca.  $30^\circ$  in solution or in vapor phase.<sup>20</sup> The phenyl–vinyl torsional barrier in the vapor phase is  $305 \text{ cm}^{-1}$  (0.9 kcal/mol), and the calculated potential energy surface is very shallow between 0 and  $45^\circ$ .<sup>18</sup> Adjacent stilbene molecules adopt an edge-to-face geometry in the solid state, whereas some donor–acceptor stilbenes adopt  $\pi$ -stacked geometries. Stilbenedicarboxamide adopts an intermediate geometry, with a  $35^\circ$  dihedral angle between the phenyl rings of adjacent stilbene molecules.<sup>18</sup> Thus, both the internal and intramolecular phenyl–phenyl dihedral angles of the stilbenes can readily adapt to optimize crystal packing.

The different conformations of hp15-1 and hp15-2 demonstrate that the ethoxy tethers do not significantly restrain the orientation of the stilbene moiety and allow both edge-to-face and parallel stacking interactions. As expected all four ethoxy tethers display *gauche* conformations around the C–C bond ( $C5'$ – $C6'$  and  $C9'$ – $C3'$ ; Figures 1, 3C). However, various combinations of torsion angles in the tethers ( $sc^+$  and  $sc^-$ ) along with subtle differences in the  $\epsilon$  and  $\zeta$  and  $\alpha$  and  $\beta$  torsions of residues G6 and C9, respectively, result in the distinct orientations seen with the Sd2 linkers here.

The parallel and edge-to-face stacking interactions in hp15-1 and hp15-2, respectively, are accompanied by subtle variations in the duplex diameters at their Sd2 ends. In hp15-1, the distance between the phosphorus atoms of S7 and C9 is 18.41 Å (av  $P \cdots P$  distance 17.91 Å). In hp15-2 the corresponding distances are both 17.66 Å. The hp15-1 and hp15-2 molecules most likely exhibit significantly different thermodynamic stability in solution, the fully stacked Sd2 linker in the former representing the low-energy form. At present, we do not have any experimental stability data for the actual conformations observed in the structure of the hp15 crystal form. However, the  $30^\circ \text{ C}$  difference

(17) (a) Lavery, R.; Sklenar, H. *J. Biomol. Struct. Dyn.* **1988**, *6*, 63–91. (b) Lavery, R.; Sklenar, H. *J. Biomol. Struct. Dyn.* **1989**, *7*, 655–667.

(18) Lewis, F. D.; Yang, J.-S.; Stern, C. L. *J. Am. Chem. Soc.* **1996**, *118*, 12029–12037.

(19) Ogawa, K.; Sano, T.; Yoshimura, S.; Takeuchi, Y.; Toriumi, K. *J. Am. Chem. Soc.* **1992**, *114*, 1041–1051.

(20) Waldeck *Chem. Rev.* **1991**, *91*, 415–536.

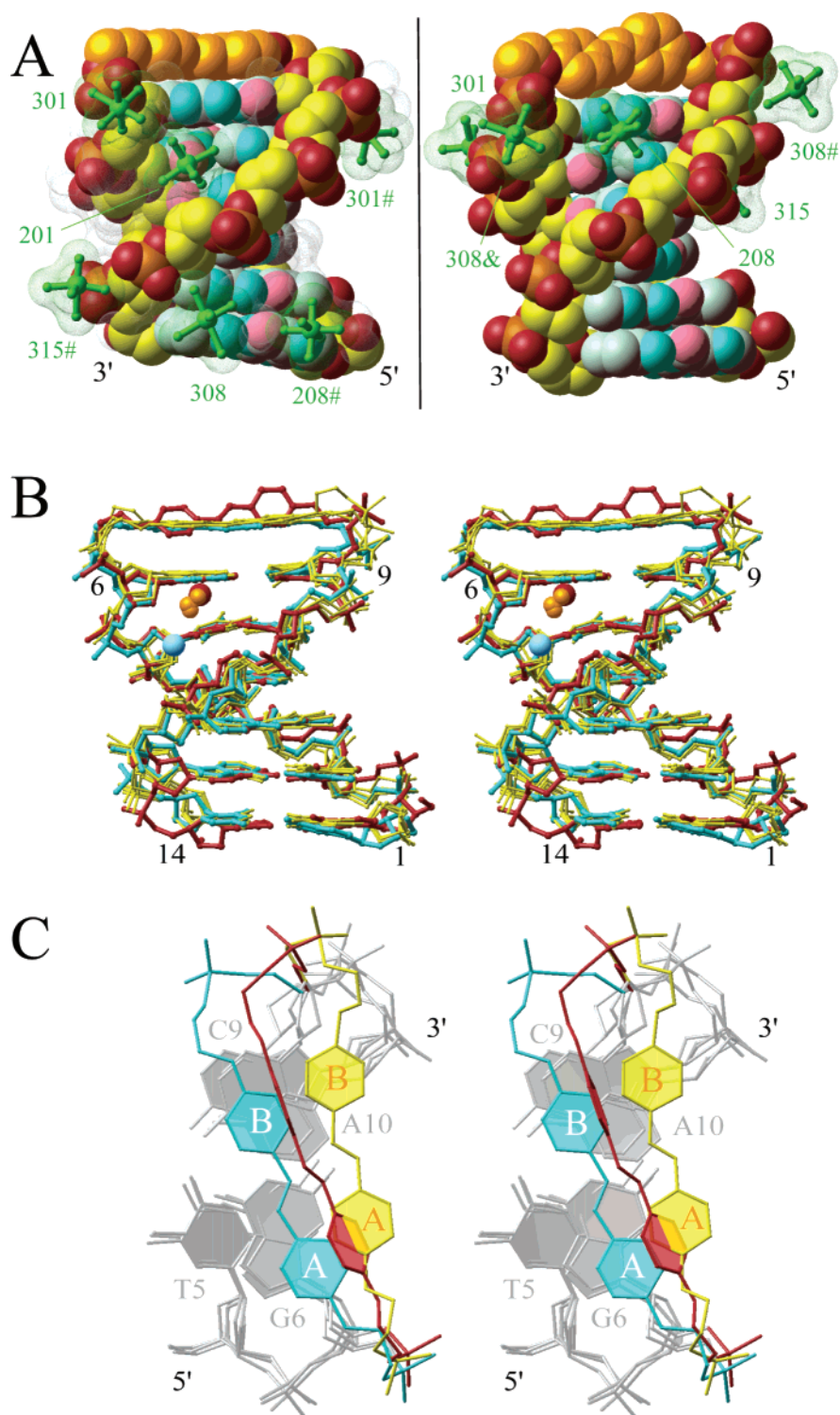


**Figure 3.** Conformations of  $d(GT_4G)$ –Sd2– $d(CA_4C)$ . (A) van der Waals representations of the structures of hp15-1 (left) and hp15-2 (right), viewed across the major and minor grooves. DNA atoms are colored yellow and light blue (backbone and base, respectively) for carbon, red and pink (backbone and base) respectively, for oxygen, blue for nitrogen, and orange for phosphorus. Sd2 linkers are highlighted in gold, and magnesium hexahydrates are shown in a ball-and-stick representation and surrounded by their Connolly surfaces. (B) Overall superposition of the hp15-1 (cyan), hp15-2 (red), and hp32-1 to hp32-4 (yellow) structures along with metal cations coordinating to the minor groove ( $Mg^{2+}$  in the hp15 crystal form and  $Sr^{2+}$  in the hp32 crystal form<sup>3</sup>). (C) Geometries and relative orientations of the Sd2 linker in hp15-1 (cyan), hp15-2 (red), and hp32-4 (yellow). The view is approximately perpendicular to the adjacent G:C base pair. The duplex portion T5:A10 and G6:C9 is shown in gray (all three structures hp15-1, hp15-2, and hp32-4 are shown), and the orientations of the linkers in hp32-1 to hp32-3 fall between those of the depicted cyan and yellow linkers.

in  $T_m$  found for duplexes  $d(T)_4$ –Sd2– $d(A)_4$  capped by *trans*- and *cis*-Sd2 linkers, respectively (the latter being unstacked),<sup>11</sup> may provide an indication of the destabilization as a consequence of disrupted parallel stacking interactions between linker

and adjacent base pair. In the hp15 crystal, the unusual conformation of the Sd2 linker in hp15-2 is stabilized by particular lattice interactions.

**Lattice Interactions.** The presence of Sd2 linkers in DNA

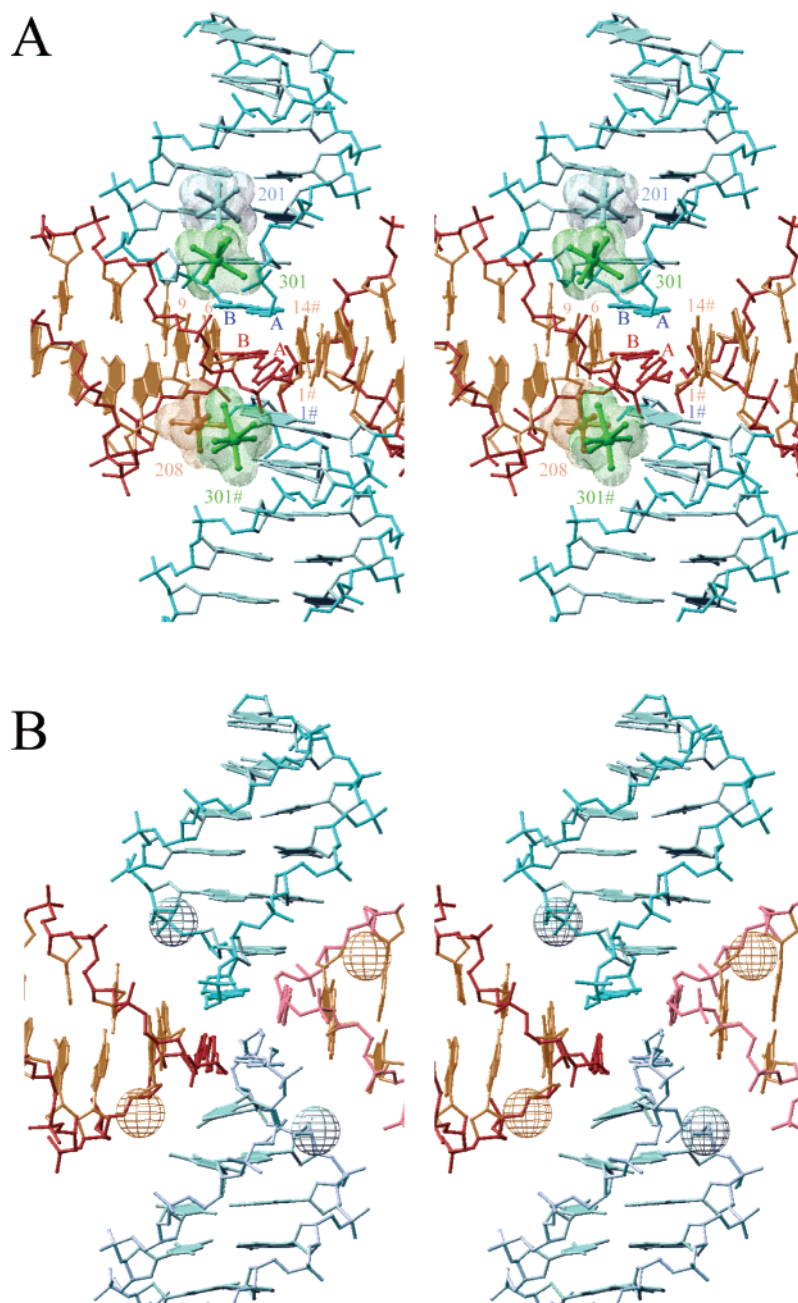


**Figure 4.** Stereo diagrams illustrating the four-way junctions mediated by Sd2 linkers in the (A) hp15 and (B) hp32 crystal forms. The color schemes are identical to those used in Figure 3B. The coloring of metal cations bound in the minor groove (Mg201 to hp15-1, cyan; Mg208 to hp15-2, red; Sr<sup>2+</sup> to hp32) match those of the individual DNA molecules. In addition, Mg301 and its symmetry mate are shown in green.

creates new types of lattice interactions. A shared feature of both crystal forms is the formation of four-way junctions. In hp15 this junction involves terminal base pairs and Sd2 linkers from both independent molecules (Figure 4A). In hp32 four Sd2 linkers are joined in a “pinwheel”-like arrangement (Figure 4B). The resulting molecular packing densities are very different for the two forms (Figure 5). The hp32 form displays large solvent channels (Figure 5B) and only limited lateral contacts between layers of duplexes (Figure 5D). This leads to a relatively high volume/base pair of 2081 Å<sup>3</sup> (counting Sd2 as a base pair). In hp15 crystals the volume/base pair is just 1142 Å<sup>3</sup> (Figure 5A). Lateral contacts between layers, mediated by Mg<sup>2+</sup> ions, are tighter in this form (Figure 5C).

At each four-way junction in hp15, separate columns of hp15-1 (shown in cyan) and hp15-2 hairpins (shown in red),

arranged head-to-tail, cross each other at nearly right angles, thereby caging the unstacked Sd2 linker of an hp15-2 molecule (Figure 4A). The resulting intermolecular edge-to-face interaction between phenyl B of Sd2 and C14# (# indicates a symmetry-related hairpin) is reminiscent of the intramolecular one between Sd2 and C9 (see section above). The distance between phenyl carbons and cytosine planes on either side of Sd2 are approximately 3.5 Å. Moreover, the dihedral angles between phenyl B and the base planes of C9 and C14# are quite similar (76° and 84°, respectively). The roof of the cage for phenyl B of the Sd2 linker in hp15-2 is formed by the deoxyribose of G1# from hp15-1 (Figures 4A, 5C). Its 4'-oxygen is directed into the phenyl ring.<sup>21</sup> The trans double bond in Sd2

(21) Egli, M.; Gessner, R. V. *Proc. Natl. Acad. Sci. U.S.A.* **1995**, *92*, 180–185.

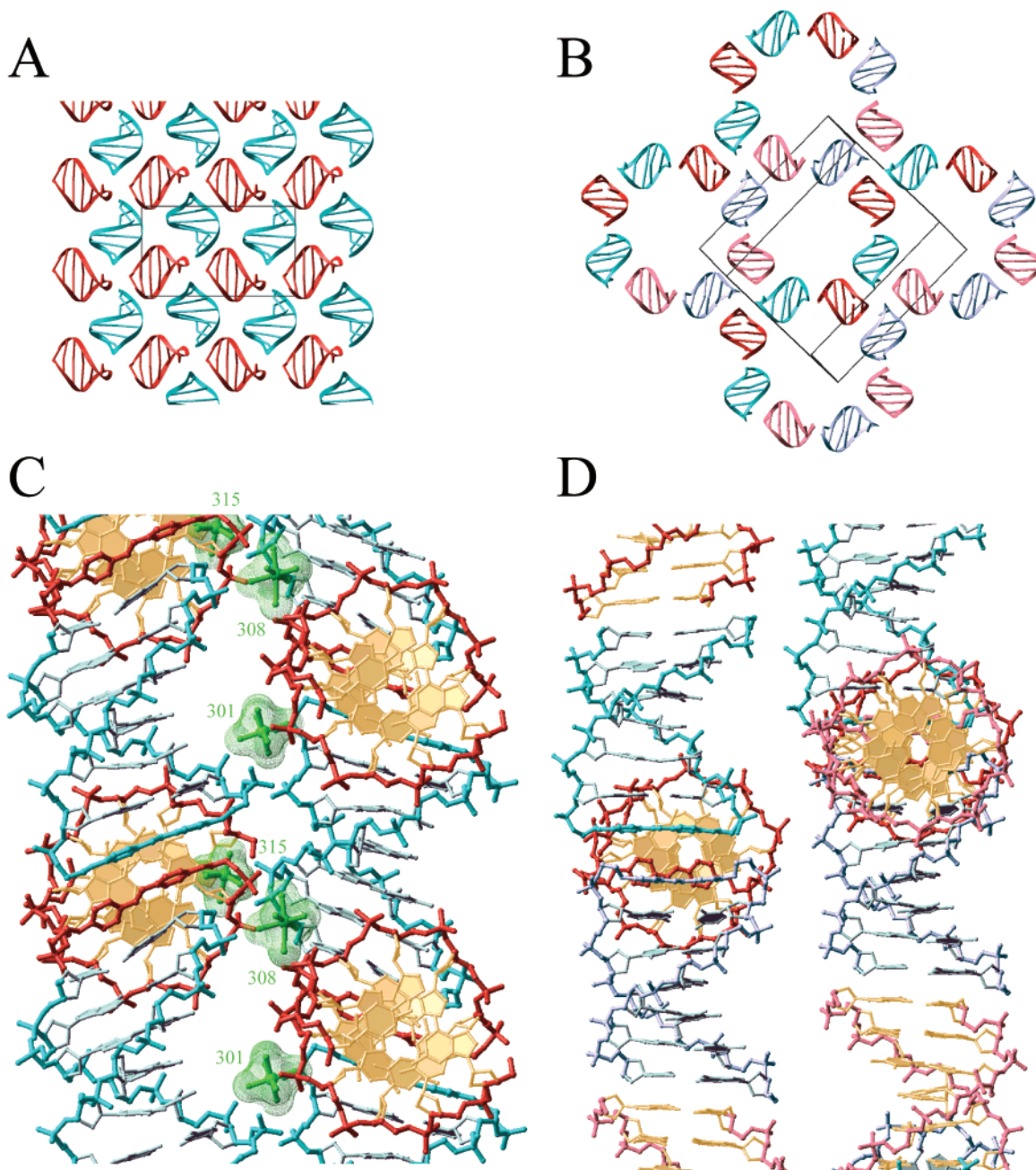


**Figure 5.** Packing modes in the hp15 and hp32 crystal forms of d(GT<sub>4</sub>G)–Sd<sub>2</sub>–d(CA<sub>4</sub>C). The orthorhombic hp15 (A) and hp32 lattices (B). Individual molecules are colored differently: Cyan (hp15-1), red (hp15-2), rose (hp32-1), cyan (hp32-2), red (hp32-3), and lavender (hp32-4). The unit cells are indicated with thin solid lines. Close-up views of the packing interactions in the hp15 (C) and hp32 crystal lattices (D). The color schemes are identical to those in panels A and B. DNA base planes are filled, and Mg<sup>2+</sup> hexahydrate complexes (green) mediating intra- (Mg301) and interlayer interactions (Mg301, Mg308, and Mg315) between duplexes in the hp15 lattice are shown in space filling mode.

from a hp15-1 molecule then constitutes the floor of the cage (Figures 4A, 5C). The distances between the 4'-oxygen and the double bond located on opposite sides of the Sd<sub>2</sub> linker along the normal to the plane defined by phenyl B are both approximately 3.4 Å. These interactions are indicative of a central role of the Sd<sub>2</sub> linker in the stabilization of the four-way junction between hairpins hp15-1 and hp15-2 and the formation of the lattice as a whole.

At the opposite end of the linker phenyl A is surrounded by three guanine bases (G6 from the same hp15-2 molecule and two G1# residues from neighboring hp15-1 and hp15-2 molecules) and phenyl A from a second hp15-1 molecule (Figure 4A). However, the conformation of that phenyl ring appears to

be considerably less constrained by its surroundings, and no parallel or edge-to-face stacking interactions are observed. The dihedral angles between the phenyl ring and the planes defined by the neighboring guanines and the second phenyl lie between 39° and 46°.

**Metal Ion Coordination.** Five ordered Mg<sup>2+</sup> ions per asymmetric unit were identified in electron density maps of the hp15 structure. All of them are hexahydrates, and therefore, all interactions between cations and stilbene hairpins are of the outer-sphere type. Details of the coordination spheres for all Mg<sup>2+</sup> ions are summarized in Table 2. Molecule hp15-1 is surrounded by six Mg<sup>2+</sup> ions (201, 208, 301, 301#, 308, and 315) and molecule hp15-2 engages in contacts to five Mg<sup>2+</sup>

**Table 2.** Mg<sup>2+</sup> Hexahydrate Coordination

cation	water	base (hp15-)	DNA ligand	distance <sup>a</sup> (Å)
Mg201 <sup>b</sup>	W1	A11 (1)	N3	2.68
		A12 (1)	O4'	2.91
	W3	T5 (1)	O2	2.69
Mg208 <sup>b,d</sup>	W1	G6 (1)	O4'	2.86
	W2	A10 (2)	N3	2.74
	W4	A11 (2)	O4'	2.95
	W5	G1#(1)	O6	2.61
	W5	G1# (1)	N7	2.69
Mg301 <sup>b,e</sup>	W3	Sd2 (1)	O1P	2.87
	W4	G6 (2)	O2P	2.66
	W5	Sd2 (1)	O1P	3.38
		Sd2 (1)	O2P	3.19
	W6	C9# (1)	O2P	2.91
		T5 (2)	O2P	2.82
Mg308 <sup>e</sup>	W2	A13 (1)	O2P	2.75
		C9# (2)	O2P	3.23
	W3	Sd2& (2)	O1P	2.78
	W4	A10# (2)	O1P	2.67
	W5	Sd2& (2)	O2P	2.54
Mg315 <sup>e</sup>	W6	C9# (2)	O1P	3.15
	W1	A10 (2)	N7	2.77
		A10 (2)	O2P	2.74
	W2	A13# (1)	O1P	2.93
		C14# (1)	O2P	2.78
W5	A10 (2)	O2P	3.15	

<sup>a</sup> Cutoff 3.5 Å. <sup>b</sup> Coordination shown in Figure 4A. <sup>c</sup> Symmetry-related nucleotides are marked by # and &. <sup>d</sup> Coordination shown in Figure 2. <sup>e</sup> Coordination shown in Figure 5C.

ions (208, 301, 308, 315, and 315#). Mg 201 is the only ion with contacts to a single DNA molecule. It is bound inside the minor groove of hp15-1 (Table 2, Figure 3A left, Figure 4) and clamps onto two adjacent base pairs of the A-tract (see section on minor groove width below). The other ions help stabilize the four-way junction or mediate lateral interactions between layers of duplexes. Mg208 resides in the minor groove of the second molecule. Compared with Mg201, it is shifted toward the Sd2 linker, and water molecules from its hydration shell form hydrogen bonds to both G6 and A10 from opposite strands (Figure 3A, right, and Figure 4A). In addition, the ion coordinates to the major groove of a symmetry-related hp15-1 molecule (N7 of G1#). Thus, Mg208 contributes to the stability of the four-way junction. Interestingly, none of the water molecules coordinated to either Mg201 or Mg208 is hydrogen bonded to a phosphate group (Table 2). Conversely, all outer-sphere contacts by Mg301, 308, and 315 (except for one interaction by Mg315, Table 2) involve exclusively phosphates. This is consistent with their role in the stabilization of the lattice. Like Mg208, Mg301 glues together four-way junctions (Figure 4A) but also mediates lateral contacts between layers of duplexes (Figure 5C). The two remaining Mg<sup>2+</sup> ions, Mg308 and Mg315, participate in the formation of lateral interactions. Of a total of 26 contacts by the five Mg<sup>2+</sup> ions (using a cutoff distance of 3.5 Å, Table 2), three involve the major groove (two H-bonds to G and one to A) and four the minor groove (two H-bonds to A and one each to G and T). The remaining 19 acceptors of hydrogen bonds by waters coordinated to Mg<sup>2+</sup> ions are either phosphates (16) or 4'-oxygens.

Recently, we found that particular locations of Mg<sup>2+</sup> and their coordination modes in the crystal structure of the Dickerson–Drew DNA dodecamer with sequence CGCGAATTCGCG are primarily a consequence of the packing and, to a lesser degree, of the sequence.<sup>22</sup> Although Mg<sup>2+</sup> ions can accentuate confor-

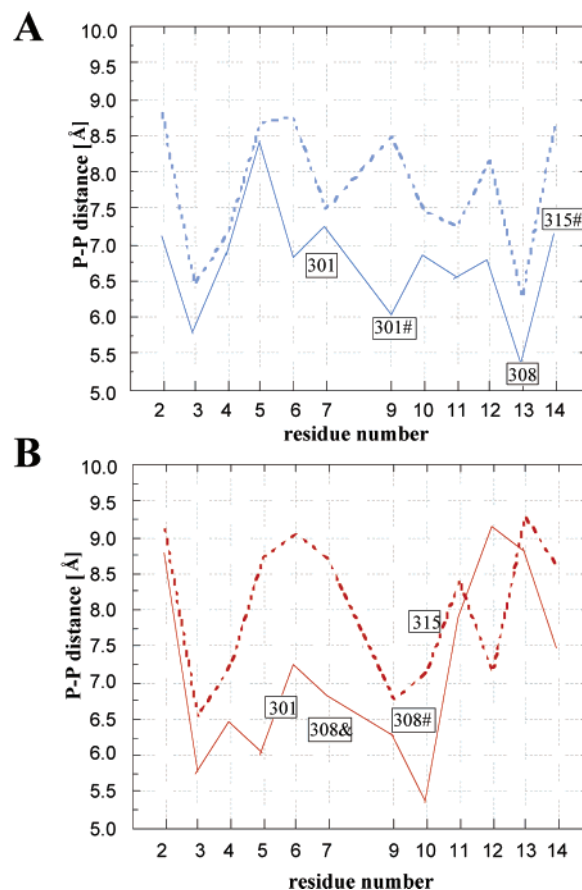


**Figure 6.** Interduplex phosphate–phosphate distances for (A) hp15-1 and (B) hp15-2. Closest and second-closest contacts are shown with solid and dashed lines, respectively, and the color codes for the Sd2 moieties match those used in Figure 3. The locations of Mg<sup>2+</sup> ions are indicated by framed residue numbers, and the symmetry operators are consistent with those given in Table 2.

mational features of the DNA 12mer in the crystal lattice, they are not at the origin of its two most distinct features, the asymmetric kink and the narrow AATT-tract minor groove.

Similarly, in the present structure of the Sd2-capped DNA hairpin, the locations of Mg<sup>2+</sup> ions 301, 308, and 315 (Table 2) are correlated with closely spaced phosphate groups from adjacent hairpins (Figure 6). Mg201 is the exception since it represents a case of a site- or sequence-specifically bound metal cation with contacts to a single DNA molecule. By comparison, a classification in terms of sequence- vs packing-related ion coordination in the case of Mg208 is somewhat more difficult. Besides binding to the minor groove of hp15-2, the ion is also engaged in a water-mediated contact to a symmetry-related hairpin molecule. Although this cation-mediated interaction between neighboring hairpins does not involve phosphate groups (Table 2), two molecules are thus required to stabilize the Mg208 binding site. Therefore, the binding mode of this ion can be viewed as both sequence- and packing specific. However, on the basis of the observation that the coordination mode within the minor groove of a single hairpin molecule is similar to that of Mg201, we may speculate that the coordination of Mg201 to hp15-1 represents a preferred binding mode of Mg<sup>2+</sup> to an

(22) Egli, M.; Tereshko, V. In *Sequence-Dependent Curvature and Deformation in Nucleic Acids and Protein-Nucleic Acid Complexes*; Stellwagen, N., Mohanty, U., Eds.; American Chemical Society Symposium Series; 2003. In press.

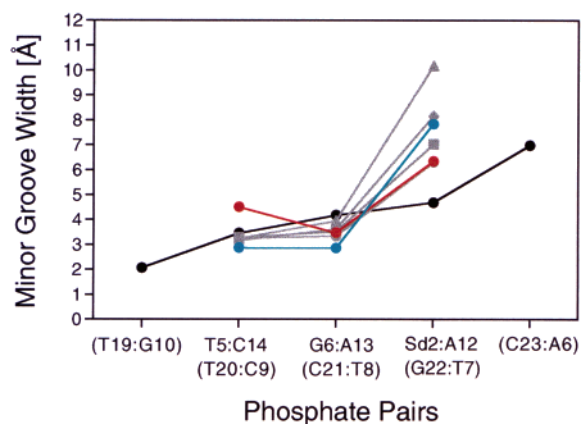


**Figure 7.** A-tract minor groove widths ( $P\cdots P$  distances  $\sim 5.8$  Å) in hp15-1 (cyan), hp15-2 (red), hp32-1 (gray squares), hp32-2 (gray triangles), hp32-3 (gray circles), hp32-4 (gray diamonds),<sup>3</sup> and the Dickerson–Drew dodecamer (DDD; black) CGCGAATTCGCG.<sup>25</sup>

A-tract minor groove in the absence of any significant packing forces.

**Geometry of the A-tract Portion.** Mg201 and Mg208 are both bound within the minor groove (Figures 3A, 4A), but their specific coordination modes lead to distinct groove topologies in hp15-1 and hp15-2. In hp15-1, the  $Mg^{2+}$  hexahydrate (Mg201) is localized inside the A-tract whereas Mg208 resides closer to the Sd2 linker in hp15-2 and contacts both G6 and A10 from opposite strands (Table 2). In the case of the Sd2-capped duplex hp15-1, the  $Mg^{2+}$  ion resides near the 5'-end of the A<sub>4</sub> stretch (Figure 3A, left). As a result the A-tract minor groove is narrower in hp15-1 relative to hp15-2 and all four hp32 molecules (Figure 7). The reduction in A-tract groove width in hp15-1 compared with that in hp15-2 amounts to between 1 and 2 Å. The hp15 structure demonstrates that a  $Mg^{2+}$  hexahydrate can penetrate the A-tract minor groove and relieve electrostatic repulsion between phosphates across the groove, thus causing significant contraction.

Detection of ordered metal cations around DNA molecules has been the focus of a multitude of studies in recent years (reviewed in ref 23). Solution NMR studies revealed penetration of the minor groove in A-tracts of the types 5'-A<sub>4</sub>T<sub>4</sub>-3' and 5'-T<sub>4</sub>A<sub>4</sub>-3' by  $Mn^{2+}$  ions.<sup>24</sup> A tandem of  $Mg^{2+}$  ions was observed to bridge opposite strands across the narrow minor groove near the end of the 5'-AATT-3' stretch in the Dickerson–Drew B-form DNA.<sup>25</sup> Moreover, binding of  $Rb^+$  at the central ApT step in the minor groove of the same DNA dodecamer was established using X-ray crystallography at high resolution.<sup>26</sup> Similarly, NMR experiments provided evidence for preferred binding of ammonium ions in the minor groove of A-tract

sequences.<sup>27</sup> However, the high-resolution structure of the Sd2-capped hairpin reveals for the first time coordination of a fully hydrated divalent metal cation inside the narrow minor groove of an A<sub>n</sub>:T<sub>n</sub> type A-tract DNA.

**Structure and Electron Transfer in Solution.** The high melting temperature of the Sd-linked hairpins indicate that they form thermodynamically stable structures in solution. Molecular mechanics calculations indicate that they adopt face-to-face geometries similar to those of hp15-1 or hp32<sup>3</sup> in solution. However, the observation of hp15-2 in the solid state suggests that the Sd linker is free to rotate about its long axis in solution. The Sd linker is strongly fluorescent in the absence of nucleobases; however, its fluorescence is strongly quenched in hairpins possessing either adjacent A:T or G:C base pairs. Fluorescence quenching is attributed to a photoinduced electron-transfer process in which singlet Sd serves as an electron donor and T or A as an electron acceptor. Femtosecond transient absorption spectroscopy has confirmed the formation of the Sd cation radical and established that both the charge separation and charge recombination processes occur on a picosecond time scale. Insertion of a G:G base pair between the Sd linker and the closest A:T base pair results in a decrease in fluorescence quenching and an increase in fluorescence lifetime. The use of G:G and other unnatural base pairs to mediate electron injection into DNA is under current investigation. The trans–cis photoisomerization of the Sd linker which occurs in the absence of nucleobases is also strongly quenched in hairpins possessing A:T or G:C adjacent base pairs. Quenching of isomerization might be attributed to either fast electron-transfer quenching or to a rigid hairpin structure which inhibits C=C torsion in the excited state. The observation of an edge-to-face geometry for hp15-2 indicates that Sd can rotate about its long axis. Thus, restricted motion seems unlikely to be responsible for the absence of photoisomerization.

**Acknowledgment.** This work was supported through grants by the National Institutes of Health to M.E. (GM55237) and by the Division of Science, Office of Basic Energy Sciences, U.S. Department of Energy to F.D.L. Portions of this work were performed at the DuPont–Northwestern–Dow Collaborative Access Team (DND-CAT) Synchrotron Research and at the Structural Biology Center (SBC-CAT) located at Sectors 5 and 19, respectively, of the Advanced Photon Source. DND-CAT is supported by the E.I. DuPont de Nemours & Co., The Dow Chemical Company, the U.S. National Science Foundation through Grant DMR-9304725, and the State of Illinois through the Department of Commerce and the Board of Higher Education Grant IBHE HECA NWU 96. SBC-CAT is supported by the U.S. Department of Energy, Office of Biological and Environmental Research, under Contract No. W-31-109-ENG-38.

(23) Egli, M. *Chem. Biol.* **2002**, *9*, 277–286.

(24) Hud, N. V.; Feigon, J. *J. Am. Chem. Soc.* **1997**, *119*, 5756–5757.

(25) Minasov, G.; Tereshko, V.; Egli, M. *J. Mol. Biol.* **1999**, *291*, 83–99.

(26) Tereshko, V.; Minasov, G.; Egli, M. *J. Am. Chem. Soc.* **1999**, *121*, 3590–3595.

JA0355527

(27) Hud, N. V.; Sklenar V.; Feigon, J. *J. Mol. Biol.* **1999**, *286*, 651–660.